

1      **Dynamics of *Teleaulax* cryptophyte prey during the decline of red water blooms**  
2                          **in the Columbia River Estuary**

3      *Authors:*

4      Maria Hamilton <sup>1,2</sup>, Gwenn M. M. Hennon <sup>1,3</sup>, Joseph Needoba <sup>4</sup>, Katie Maxey <sup>4</sup>, Rhonda Morales <sup>1</sup>,  
5      Tawnya D. Peterson <sup>4</sup>, Megan Schatz <sup>1</sup>, Jarred Swalwell <sup>1</sup>, Peter Zuber <sup>4</sup>, E. Virginia Armbrust <sup>1</sup>,  
6      Francois Ribalet <sup>1\*</sup>

7  
8      *Affiliations:*

9  
10     <sup>1</sup> School of Oceanography, University of Washington, Box 357940, Seattle, WA 98195 USA

11     <sup>2</sup> Present address: Ocean Sciences Department, UC Santa Cruz, 1156 High Street, Santa Cruz, CA  
12     95064

13     <sup>3</sup> Lamont-Doherty Earth Observatory, Columbia University, 61 Route 9w, Palisades, NY 10964

14     <sup>4</sup> Institute of Environmental Health, Oregon Health & Science University, 3181 SW Sam Jackson  
15     Park Rd., Portland, OR 97239 USA

16

17     \* Corresponding author: [ribalet@uw.edu](mailto:ribalet@uw.edu)

18

19 ABSTRACT

20 The mixotrophic *Mesodinium major* is a globally distributed nontoxic ciliate that relies on the  
21 acquisition and use of chloroplasts derived from its cryptophyte prey, *Teleaulax amphioxeia*. The  
22 ecology and physiology of the *T. amphioxeia* prey is not well known, nor is it clear how their growth  
23 influences the dynamics of *M. major* blooms, which turn the water red. A 4-week survey was  
24 conducted in the Columbia River estuary in 2013 during the decline of red water blooms to better  
25 understand how environmental factors influence the population dynamics of *T. amphioxeia*.

26 Abundances and division rates of free-living *Teleaulax*-like cryptophytes were continuously monitored  
27 using flow cytometry. The highest abundance of cryptophytes occurred during the first neap tide with  
28 concentrations as high as  $1.8 \times 10^6$  cells L<sup>-1</sup> and decreased during spring tide and later neap tides ( $< 0.5$   
29  $\times 10^6$  cells L<sup>-1</sup>). A 10-fold variation in cryptophyte abundances occurred daily, which was not  
30 associated with the daily tidal cycle or the spring/neap tide cycle. Cryptophyte division rates, estimated  
31 *in situ* for the first time, ranged from 0.2 to 1.5 d<sup>-1</sup>, with the highest rates observed in accordance with  
32 high abundances of *Teleaulax*-like cryptophytes. These division rates were positively correlated with  
33 concentrations of dissolved inorganic nitrogen and phosphorus, suggesting nutrient availability, rather  
34 than light conditions, limits the growth of *T. amphioxeia* at that time. Assuming a minimum ingestion  
35 rate of  $\sim 1$  cryptophyte ciliate<sup>-1</sup> day<sup>-1</sup>, our results suggested that the growth of *M. major* was limited by  
36 prey availability during the survey.

37

38 Key words: cryptophytes; *Teleaulax*; *Mesodinium*; growth rates; SeaFlow.

39 INTRODUCTION

40 The common coastal ciliate, *Mesodinium major* was previously included in the *Mesodinium*  
41 *ruberum* (*Myrionecta rubra*) (Lohmann 1908) Jankowski 1976 species complex (Garcia Cuetos et al.  
42 2012) and is among the marine microzooplankton that temporarily maintains the plastids of their  
43 cryptophyte algal prey, *Teleaulax amphioxeia* (Herfort et al. 2011). This association allows the ciliate  
44 to function as a mixotroph, capable of utilizing both phagotrophy and photosynthesis to acquire carbon  
45 (Crawford 1989). Although *M. major* populations are important primary producers in many coastal and  
46 estuarine systems (Stoecker et al. 1989, Herfort et al. 2012), little is known about the ecology and  
47 physiology of the *T. amphioxeia* prey and how their growth and abundance may influence bloom  
48 dynamics.

49 Massive *M. major* blooms occur each summer in the Columbia River estuary (Herfort et al.  
50 2011). The blooms persist for several weeks during the late summer and early fall, and shift the trophic  
51 status of the estuary from net heterotrophic to net autotrophic (Herfort et al. 2012). The annual *M.*  
52 *major* bloom appears to be initiated during summer neap tides (Herfort et al. 2011), when both tidal  
53 forcing and the seasonality of freshwater discharge result in an extended summer saltwater intrusion  
54 (Chawla et al. 2008). The blooms appear to start in Baker Bay, where a shallow depth and long water-  
55 retention time favor the persistence of high cell abundances ( $>100$  cells  $\text{mL}^{-1}$ ) and fast division rates  
56 ( $1.2\text{--}3.1 \text{ d}^{-1}$ ) of *M. major*. Within a few weeks, the initial blooms spread throughout the main estuary  
57 (Herfort et al. 2011). A decline in the abundance of small ( $<5 \mu\text{m}$ ), free-living *Teleaulax* cells  
58 coincided with an increase in *M. major* abundance observed in the estuary in 2011 (Peterson et al.  
59 2013), suggesting a direct link between consumption of the cryptophyte prey and the initiation of *M.*  
60 *major* blooms. Further evidence of a connection between prey populations and the development of  
61 *Mesodinium* blooms was observed in an Antarctic saline lake, where an increase in the abundance of  
62 cryptophytes preceded the increase in abundance of *M. rubrum* (van den Hoff & Bell 2015). However,  
63 the factors that influence cryptophyte prey population dynamics remain poorly understood in these

systems, and the underlying mechanisms linking ciliate and prey populations are unclear. For example, does the physiological status of free-living cryptophyte prey (as indicated by division rate rather than population size) influence the dynamics of *Mesodinium* blooms?

To investigate the influence of prey population size and physiological status on the dynamics of *Mesodinium* blooms, we examined patterns in abundances and division rates for free-living *T. amphioxiae*. Numerous factors influence cell abundances, including cell division and cell mortality, and physical advective transport. In a dynamic system such as the Columbia River estuary, only a continuous sampling approach can capture changes in abundances over time. Continuous measurements of the population size structure can be used to estimate division rates based on changes in cell size distribution over the course of a day (Sosik et al. 2003, Hunter-Cevera et al. 2014, Ribalet et al. 2015). This method eliminates many of the difficulties and biases associated with the determination of cell division rates using discrete sampling techniques (Laws 2013).

Here, we use the continuous flow cytometer, SeaFlow (Swalwell et al. 2011) to determine cryptophyte abundances and division rates both in the laboratory and during a 4-week survey carried out in 2013. Dissolved nutrient concentrations, salinity, temperature, light irradiance, and abundances of cryptophytes and *M. major* were determined during red water blooms in the Columbia River estuary. Daily division rates of cryptophytes were calculated from the change of size distribution over a 24-h period using a size-structured division rate model (Ribalet et al. 2015). The abundance and division rates of cryptophyte populations were compared with abundances of *M. major* to determine the influence of prey physiology and abundance on the dynamics of red water blooms.

84

85

## 86 METHODS

### 87 Study Area

88 Samples were collected at 2.4 m depth for 1 month, 4 days a week, from September 11<sup>th</sup> to

89 October 2<sup>nd</sup> 2013 from a continuous seawater flow-through system at SATURN-03, a fixed station  
90 located at the end of a dock in Hammond, OR (**Fig. S1**) (Baptista et al. 2015). Discrete samples were  
91 also collected at the station during the turn of the high tide (i.e., at slack water).

92

### 93 **In situ monitoring**

94 Water temperature and salinity were measured at SATURN-03 using a SeaBird 37  
95 Conductivity-Temperature (CT) meter deployed in-line with the pumped water system described in  
96 Baptista et al (2015) that alternates between 3 depths. For this study, water measurements were  
97 extracted for the 2.4-m depth corresponding to the flow cytometry sampling described below. Water  
98 temperature and salinity were measured continuously at SATURN-03 using a SeaBird Conductivity-  
99 Temperature (CT) meter for temperature and salinity, and a chlorophyll fluorometer (Turner designs).  
100 Photosynthetic Active Radiation (PAR) data was obtained from Desdemona Sands Light mooring,  
101 located 3 km north of SATURN-03.

102

### 103 **Inorganic nutrients**

104 Duplicate nutrient samples were collected from water pumped to the surface at SATURN-03,  
105 collected in temporary bottles and then filtered into 30 ml HDPE storage bottles. All bottles for  
106 collection and storage of samples, syringes, and filter housings were washed with 10 % hydrochloric  
107 acid and rinsed 3 times with deionized water before use. Bottles, syringes, and filter housings were  
108 dried, capped, and stored in clean Ziploc bags until use. Collection bottles were rinsed three times with  
109 sample and filled by gently pushing sample through a clean Swinnex filter holder and combusted 25-  
110 mm glass fiber filter (Whatman GF/F) using a clean 60-ml syringe. Storage bottles were rinsed three  
111 times with filtered sample before final filling; samples were frozen upright at -20 °C.

112 Nutrient concentrations were determined using an Astoria Analyzer (Astoria-Pacific, Clackamas,  
113 OR, USA). Before analysis, all samples were thawed in a water bath (55 °C) and cooled to room

114 temperature. Nitrate, nitrite, ammonium, and orthophosphate were determined using manufacturer  
115 recommended methodology (Armstrong et al. 1967), EPA 1984, EPA 1997). These methods have  
116 minimum detection limits (MDL) of 0.5, 0.2, 0.3, 0.2  $\mu\text{M}$ , respectively. Quality assurance was  
117 maintained by running certified reference material (ERA catalog #4023).

118

119 **Determination of cryptophyte cell abundance and cell size**

120 Continuous measurements of cryptophyte abundances and cell size were made using SeaFlow  
121 (Swalwell et al. 2011). The instrument was equipped with a 457-nm 300-mW laser (Melles Griot).  
122 Forward light scatter (a proxy for cell size), red, and orange fluorescence were collected using a 457–  
123 50 bandpass filter, 692–40 band-pass filter, and 572–27 bandpass filter, respectively. Seawater was  
124 prefiltered through a 100- $\mu\text{m}$  stainless steel mesh (to eliminate large particles) prior to analysis. The  
125 flow rate of the water stream was set at 15  $\text{mL min}^{-1}$  through a 200- $\mu\text{m}$  nozzle. A programmable  
126 syringe pump (Cavro XP3000, Hamilton Company) continuously injected fluorescent microspheres (1  
127  $\mu\text{m}$ , Polysciences) into the water stream as an internal standard. Files were written every three minutes.  
128 Data were analyzed using the R package *Popcycle* version 0.2 (available on GitHub). A sequential  
129 bivariate manual gating scheme was used to cluster the cryptophyte population based on forward light  
130 scatter, orange and red fluorescence measurements.

131 To confirm the identification of cryptophyte cells, discrete samples for flow cytometry were  
132 collected once a day during slack tide, fixed with 0.025% glutaraldehyde and stored at -80 °C. Six  
133 months after sample collection, fixed samples were analyzed with a BD Influx cell sorter equipped  
134 with a 488-nm 200-mW laser (Coherent). One hundred cells from the gated population with high  
135 orange fluorescence and high red fluorescence (assumed to represent phycoerythrin-containing  
136 cryptophyte cells) were sorted onto a glass slide. Sorted cells were then examined under a Nikon  
137 Eclipse 80i epifluorescence microscope at 400x magnification and photographed using a Qimaging  
138 MicroPublisher 3.3 RTV camera.

139 We estimated cryptophyte cell size using an empirical relationship between light scatter measured  
140 by SeaFlow and cell size measured by a Coulter Counter for different exponentially growing  
141 phytoplankton cultures of cell sizes ranging from 1 to 10  $\mu\text{m}$  (Ribalet et al. 2015).

142

143 **Estimates of cryptophyte cell division rates**

144 *Laboratory culture validation*

145 A non-axenic culture of the cryptophyte *Rhodomonas* sp. (CCMP 755) was grown in the  
146 laboratory in natural seawater amended with f/2 nutrients at 13 °C with a 16:8 light-dark cycle of 100  
147  $\mu\text{mol photons m}^{-2} \text{s}^{-1}$  provided by white fluorescent tubes. The culture was grown for 4 d in a 20-L  
148 batch culture and continuously mixed with a magnetic carboy stir bar. A peristaltic pump (Peri-Star Pro,  
149 World Precision Instruments) collected samples at a rate of 15 mL min<sup>-1</sup> for 15 min every hour for  
150 measurement with SeaFlow. On day 3, 1 mL samples of the culture were collected in triplicate every 2  
151 h for 28 h, fixed with 0.01% glutaraldehyde and stored in liquid nitrogen for cell-cycle analysis. One  
152 month after sample collection, fixed samples were stained with the green-fluorescing DNA stain SYBR  
153 Green I (diluted with dimethylsulfoxide) at a final concentration of 0.01% for 15 min at room  
154 temperature in the dark. Following the addition of fluorescent microspheres (1  $\mu\text{m}$ , Polysciences) used  
155 as an internal standard, stained samples were analyzed with a BD Influx flow cytometer. Data were  
156 obtained using the *Spigot Operating Software* version 5.0 (BD Biosciences) and analyzed using *FlowJo*  
157 version 9.7.2 (Tree Star). At least 10,000 cells were collected per sample. DNA frequency distributions  
158 were analyzed using the *FlowJo* cell cycle platform to obtain cell fractions in G1, S, and G2+M phases.  
159 Division rates based on DNA distributions were computed as described previously (Carpenter & Chang  
160 1988). Cell-cycle based estimates of division rates were then compared with size-structure modeled  
161 division rates.

162

163 *Size-structured matrix model*

164 We used a size-structured matrix population model developed by Sosik et al. (2003) to estimate  
165 cryptophyte population division rates. The model represents changes in cell sizes over a diel cycle and  
166 can be fit to time series of cell size distribution. The fitted model provides an estimate of the daily  
167 division rate independently from cell abundance. We implemented Sosik's original Matlab model in an  
168 R package *ssPopModel* version 0.1.1, available on Github. The model is based on the assumptions that  
169 1) cell growth is determined by light exposure, with other abiotic factors such as nutrient availability  
170 and temperature operating at longer time scales, 2) the probability of a cell dividing depends on size, 3)  
171 all cells within a discrete size class have the same probability to change to another size class, and 4) a  
172 cell divides into two daughter cells, each half the size of the mother cell. The model predicts the cell  
173 size distribution over the course of the day using the cell size/cell division relationships and the light-  
174 dependence of cell division. Daily-averaged division rates were calculated as the sum of hourly  
175 division rates over a 24-h period. The formulation and details of the model can be found in Ribalet et al.  
176 (2015).

177

## 178 **Cryptophyte community composition**

### 179 *DNA extraction*

180 Sample volumes of 0.5-2.0 L were size fractionated with a 20 µm filter followed by a 0.2 µm  
181 Sterivex filter to separate the *Teleaulax* symbiont in *M. major* cells from free living *Teleaulax*. Filters  
182 were fixed with 2 mL of RNAlater and stored at -80°C until extraction. DNA were extracted using the  
183 CTAB method (Li et al. 2013). Extracted DNA was purified using a DNA Clean and Concentrate Kit  
184 (Zymo Research). The total extracts were stored at -20°C until further use.

185

### 186 *Identification of the cryptophyte nuclear 28S D2 unique sequence element*

187 The Unique Sequence Element (USE) found in the D2 region of the LSU (28S) rRNA sequence  
188 of around ~ 220 bp was used to distinguish between *T. amphioxiae* and other free-living cryptophytes

189 (Kahn et al. 2014). Primers (crp28SF CTTGCTTGGGAATGCAGGTC /crp28SR  
190 TACGAGCCTCCACCAGAGTT) were used to PCR amplify the LSU D2 of *Teleaulax*. Single-cell  
191 PCR was performed on *M. major* cells from red water in the estuary collected in 2011 and 2014. The  
192 Antarctic strain of *M. rubrum* (CCMP2563) fed with the cryptophyte *Geminigera cryophilus* (CCMP  
193 2564) served as a control. The PCR protocol for the LSU D2 sequence identification was as follows:  
194 initial denaturation at 95 °C for 3 min; 35 cycles of denaturation at 95 °C for 45 s, annealing at 50 °C  
195 for 40 s, and extension at 70 °C for 2 min; and a final extension at 70 °C for 7 min. The resulting PCR  
196 products were purified (UltraClean PCR clean up kit, MoBio), ligated into a TOPO 2.1 vector  
197 (Invitrogen), and transformed into chemically competent *E. coli* cells (DH5 $\alpha$  strain). DNA from  
198 transformants were extracted (FastPlasmid Mini Kit, 5 Prime) and samples were sent to the Molecular  
199 and Cellular Biology Core of the ONPRC for sequencing. Sequences of around 650 bp were assembled  
200 and aligned using *Geneious* software version 7.0.6.

201

## 202 *Real Time PCR*

203 The relative proportions of cryptophyte populations and of the specific prey populations (*T.*  
204 *amphioxiaeia*) were monitored in environmental samples by qPCR. Quantitative PCR was performed on  
205 a StepOnePlus Real Time PCR system (Life Technologies) using SYBR Green as the reporter dye and  
206 the following protocol: initial denaturation at 95 °C for 10 min; 40 cycles of denaturation at 95°C for  
207 15 s, and extension and data acquisition at 60 °C for 1 min; followed by a melting curve analysis  
208 (Zuber et al., in preparation). The *T. amphioxiaeia* specific primers [TxD2 1F  
209 (TGAAAAAAGGCCTGAAATTG) /TxD2 USE 2R (ATCATTCACTCGCATGCCCC)] were used to  
210 amplify the USE of the prey cryptophyte. General cryptophyte primers targeting sequences from a  
211 region downstream of the USE [CrpSpecf 3F (GTTCTGAAGATGCTGGCACCA)/ CrpSpecf 3R  
212 (GTTCTGAAGATGCTGGCACCA)] were used to monitor cryptophyte populations and calculate the  
213 ratio of amplicons from *T. amphioxiaeia* to cryptophytes. Primers were designed using Primer-BLAST

214 from NCBI and confirmed with PCR.

215       The Antarctic *M. rubrum* culture was used as a control (i.e., negative for prey-specific and  
216 positive for general-cryptophyte sequences). Standards, samples and water blanks were analyzed in  
217 triplicate with 1 µL of 10-fold diluted DNA template added in each reaction. Standards for qPCR were  
218 constructed with the cloned *T. amphioxiae* LSU D2 region, which contained both *T. amphioxiae*  
219 specific USE and general cryptophyte sequences. A standard curve was generated from six standards  
220 with concentrations ranging from  $9.289 \times 10^6 - 9.289 \times 10^1$  D2 copies  $\mu\text{L}^{-1}$ . The number of gene copies  
221 in the standard and samples were calculated as described previously (Kahn et al. 2014).

222

### 223 ***Mesodinium major* cell abundance**

224       Forty-five mL samples fixed with a final concentration of 0.5% glutaraldehyde were collected  
225 into 50 mL centrifuge tubes for *M. major* counts and stored at -20 °C. Prior to analysis, the samples  
226 were slowly thawed to 4 °C and analyzed using an imaging flow cytometer (FlowCAM, Fluid Imaging,  
227 Inc.). A minimum of 1000 particles with diameter >5 µm was captured and the images were filtered  
228 using *VisualSpreadsheets* software version 3.1 (Fluid Imaging, Inc.) according to size. Those  
229 resembling *M. major* were selected based on visual inspection and enumerated. Flow rates were  
230 calculated using *VisualSpreadsheets* software, allowing for the quantification of cellular abundances.

231

## 232 **RESULTS**

### 233 **Environmental conditions**

234       The Columbia River estuary is a turbid and often highly stratified system characterized by  
235 dynamic physical processes, short water retention time (0.5-5 d), and strong influence from diurnal and  
236 semi-diurnal tides (Neal 1972, Jay & Smith 1990). Throughout the 4-week survey at SATURN-03 (**Fig.**  
237 **S1**), surface water (2.4-m depth) temperature and salinity were anti-correlated and oscillated with the  
238 tidal cycle, with high tide characterized by colder, higher salinity water from the Pacific Ocean, and

239 low tide characterized by warmer, lower salinity water from the Columbia River (**Fig. 1A**). The survey  
240 began and ended during the neap tide period of the mixed semidiurnal tidal cycle (day 1-7, day 14-25).  
241 The spring tide, which occurred during the second week of the survey (day 7-14), coincided with the  
242 largest oscillations in surface water salinity and temperature observed during the survey. The lowest  
243 average salinity was observed on the last neap tide (day 23-25), and corresponded to little variation in  
244 temperature (**Fig. 1A**).

245 Chlorophyll *a* concentration, a proxy for phytoplankton biomass, was high the week before the start  
246 of the survey ( $>2 \mu\text{g L}^{-1}$ ) and decreased later on (**Fig. 1B**). The lowest values during the survey were  
247 observed during neap tides (day 1-7, day 14-25), and increased during spring tide (day 7-14). A  
248 positive correlation between chlorophyll *a* concentrations and tidal cycle was observed during the  
249 survey, with high chlorophyll corresponding to high salinity ( $R = 0.58$ ,  $p < 0.001$ ). Percent saturation  
250 of oxygen showed a similar pattern to chlorophyll *a* concentrations, with the highest saturation  
251 observed before the start of the survey ( $> 90\%$ ), and reduced saturation during neap tides (**Fig. 1B**).

252 Concentrations of dissolved inorganic nitrogen (DIN as the sum of nitrate, nitrite and ammonium)  
253 and dissolved inorganic phosphate (DIP) were relatively high during the survey ( $> 5 \mu\text{M}$  and  $> 0.4 \mu\text{M}$   
254 for DIN and DIP, respectively), with the highest values observed at day 7, coinciding with the start of  
255 the spring tide (**Fig. 1C**). DIN and DIP concentrations co-varied throughout the survey.

256

## 257 **Cell abundances**

258 Fixed samples of putative cryptophyte populations with characteristic size and orange fluorescence  
259 were examined under a light microscope after sorting with a BD Influx flow cytometer (**Fig. 2A**). The  
260 small size ( $<5 \mu\text{m}$  in length) and teardrop shape of the cells (**Fig. 2B**) corresponded with previous  
261 observations of *Teleaulax amphioxiae* cells (Peterson et al. 2013), suggesting that the cryptophyte cell  
262 population measured by the SeaFlow during the survey corresponded to a *T. amphioxiae* population.  
263 Quantitative PCR was used to determine the abundance of *T. amphioxiae* ribosomal DNA copy number

relative to the abundance of total cryptophyte ribosomal DNA copy number. Based on this analysis, *T. amphioxiae* was always less than 1% (0.06% to 0.40%) of all cryptophyte sequences, with the highest and lowest percentages of *T. amphioxiae* occurring during the first and second week of the survey, respectively (**Table S1**). This result, in combination with cell sorting, suggested that > 99% of cryptophytes detected by qPCR was not quantified by the cytometer, probably because most cryptophyte cells were larger than the size range of the SeaFlow instrument (0.5 to 15  $\mu\text{m}$ ).

270

Hourly-averaged cell abundances of *Teleaulax*-like cryptophytes measured continuously by flow cytometry ranged from  $0.02 \times 10^6$  to  $1.8 \times 10^6$  cells  $\text{L}^{-1}$ , with an average of  $0.29 \times 10^6$  cells  $\text{L}^{-1}$  (**Fig. 3**). Cell abundances obtained with the SeaFlow were in excellent agreement with discrete samples analyzed by conventional flow cytometry ( $R^2 = 0.83$ ,  $p < 0.01$ , **Fig. S2**). Discontinuity in cell abundance resulted when the flow cytometer clogged due to high concentrations of suspended particle in the water. The highest abundances were observed during the first two days of the first neap tide, with a daily averaged abundance of  $0.52 \times 10^6$  cells  $\text{L}^{-1}$ , (**Fig. 3A**). The spring tide (days 7-14) and second two neap tides (days 14-25) exhibited the lowest abundances, with an average of  $0.08 \times 10^6$  cells  $\text{L}^{-1}$  and  $0.09 \times 10^6$  cells  $\text{L}^{-1}$ , respectively (**Fig. 3B and C**). Although variations in cell abundance changed rapidly over a few hours, changes in the abundance of *Teleaulax*-like cells did not coincide with daily tidal cycle or spring/neap tide cycle.

282

The abundances of *M. major* (measured once a day at high-tide) were on the same order of magnitude, but typically lower than abundances of *Teleaulax*-like cryptophytes detected by the flow cytometer, with values varying from  $0.021 \times 10^6$  to  $0.32 \times 10^6$  cells  $\text{L}^{-1}$  during the survey (**Fig. 3**). A positive correlation between abundances of *Teleaulax*-like cryptophytes and *M. major* was observed during the survey ( $R = 0.49$ ,  $p < 0.01$ ) (**Fig. 4**). Note that the only observation that does not follow the trend is when *M. rubra* is at its highest cell abundance. Abundances of *M. major* and *Teleaulax*-like

289 cells were not significantly correlated with environmental conditions such as salinity, nutrient  
290 concentrations or spring/neap tide cycle during the survey (data not shown).

291

292 **Division rates**

293 To gain confidence that size distribution data from SeaFlow could accurately estimate division  
294 rates of natural populations of cryptophytes, we compared size-based estimates of division rates ( $\text{h}^{-1}$ )  
295 with cell-cycle based estimates of division rates for *Rhodomonas* in culture, a cryptophyte of similar  
296 size range as *T. amphioxiae* (6-12  $\mu\text{m}$  in diameter). The hourly division rates estimated using DNA-  
297 based cell cycle analyses and the size-structured model provided similar range of estimate division  
298 rates and followed the same general trend throughout the experiment (**Fig. 5**), although some  
299 significant differences occurred around dawn (at hour 1, 3 and 27). The coefficient of determination  $R^2$   
300 = 0.60 ( $p < 0.001$ ) (**Fig. S3**) indicated that the model provided reasonable estimates of division rates for  
301 the cryptophyte *Rhodomonas* in culture. Restricted access to the sampling site in the field prevented  
302 use of the cell-cycle method, which requires discrete samples taken at least every 2 hrs over the 24-hr  
303 cycle. Instead, division rates for the *Teleaulax*-like cryptophyte population were derived from model-  
304 based estimates. During the survey, the median size of the *Teleaulax*-like cryptophyte population  
305 increased during daylight and decreased at night, regardless of the tidal cycle (**Fig. 6A**), which is  
306 consistent with the model assumptions that photosynthesis and cell division are the main factors  
307 influencing the change of cell volume over a 24-h period (Sosik et al. 2003).

308

309 Estimates of the daily division rates of *Teleaulax*-like cryptophyte population during the survey  
310 ranged from  $0.2 \pm 0.1 \text{ d}^{-1}$  to  $1.5 \pm 0.1 \text{ d}^{-1}$ , equivalent to 0.3 and 2.1 division per day, respectively, with  
311 the highest division rate observed on day 3 (**Fig. 6B**). Division rates were positively correlated with  
312 concentrations of dissolved inorganic nutrients ( $R = 0.66$  and  $0.55$ ,  $p < 0.05$ , for DIP and DIN,  
313 respectively) (**Fig. 7**). No significant correlation was observed between division rates and other

314 environmental factors, such as temperature or PAR (data not shown).

315

## 316 DISCUSSION

### 317 Ecophysiology of the *Teleaulax amphioxeia* during the survey

318 The cryptophyte *Teleaulax amphioxeia* is a cosmopolitan marine species that is widely  
319 distributed in coastal habitats worldwide. During our survey, *Teleaulax*-like cryptophyte abundances  
320 shifted dramatically over the course of just a few hours (**Fig. 3**), suggesting that *T. amphioxeia*  
321 distribution is very patchy within the estuary, likely due to strong physical transport. Such variability in  
322 cell abundance over short time scales emphasizes the importance of continuous measurements, such as  
323 continuous flow cytometry, for monitoring phytoplankton in estuaries. No consistent increase in  
324 cryptophyte cell abundance was observed with seawater intrusion (**Fig. 3**), and variations in  
325 abundances were not directly related to the daily tidal cycle or spring/neap tide cycle. The lack of a  
326 relationship between *Teleaulax*-like cryptophyte cell abundance and salinity is in direct contrast with  
327 our measurements of chlorophyll *a* concentrations (**Fig. 1B**), which suggests that seawater intrusions  
328 bring into the estuary many phytoplankton cells of marine origin.

329

330 Despite its patchy distribution, *Teleaulax*-like cryptophytes were always detected throughout  
331 the survey, enabling us to estimate division rates of *Teleaulax*-like cryptophyte population for the first  
332 time in the field (**Fig. 6**). The highest estimates of division rates for *Teleaulax*-like cryptophyte  
333 population reached  $1.5 \text{ d}^{-1}$  during the survey (day 3), which is consistent with previously observed  
334 division rates for isolates grown in the laboratory under nutrient replete conditions (Nishitani et al.  
335 2008, Rial et al. 2013). This results suggests that, at that time, *T. amphioxeia* was growing near optimal  
336 growth conditions. The positive correlation between division rates of the cryptophyte and  
337 concentrations of dissolved inorganic nitrogen and phosphorus ( $R = 0.55$  and  $0.66$ ,  $p < 0.05$ , for DIN  
338 and DIP, respectively) (**Fig. 7**), suggested that nutrient availability controlled division rates of *T.*

339 *amphioxiae* during the survey. The potential effect of nutrient availability on *T. amphioxiae* growth is  
340 unexpected in the turbid waters of the Columbia River estuary, where light is generally considered to  
341 be an important factor limiting phytoplankton growth (Small et al. 1990). No significant correlation  
342 between photosynthetically active radiation (PAR) and *T. amphioxiae* division rates was observed  
343 during the survey (data not shown), which supports previous studies that hypothesized that the  
344 photosynthetic machinery of cryptophytes is well adapted to low-light conditions (Bergmann et al.  
345 2004).

346

347 **Influence of *Teleaulax* cryptophyte abundances on *M. major***

348 Abundances of *Teleaulax*-like cryptophytes during our survey were comparable to previous  
349 year estimates in the estuary, with abundances ranging from 0.1 to  $1 \times 10^6$  cells L<sup>-1</sup> (**Fig. 3**) (Peterson et  
350 al. 2013) while abundances of *M. major* remained low ( $<0.3 \times 10^6$  cells L<sup>-1</sup>) (**Fig. 3**) as compared to the  
351 high number ( $> 8 \times 10^6$  cells L<sup>-1</sup>) observed at the surface (1-2 m) during red water blooms (Peterson et  
352 al. 2013). High chlorophyll *a* concentrations in fall ( $> 2 \mu\text{g L}^{-1}$ ), such as those observed before the start  
353 of the survey (**Fig. 1**), are associated with *M. major* blooms in the Columbia River estuary (Herfort et  
354 al. 2012). The sharp decline and subsequent low chlorophyll *a* concentrations suggests that the survey  
355 took place during the decline of *M. major* blooms.

356 The reason for the decline in *M. major* abundance remains unclear. The abundances of  
357 *Teleaulax*-like cryptophytes were very similar to those of *M. major* during the survey, except at the  
358 peak of *M. major* abundance where low abundance of *Teleaulax*-like cryptophytes was observed (**Fig.**  
359 **4**), suggesting that *M. major* exert a strong impact on cryptophyte prey populations. The correlation  
360 between *Teleaulax*-like cryptophytes and *M. major* abundances suggests a tightly-coupled predator-  
361 prey relationship. Assuming an ingestion rate of  $\sim 1$  cryptophyte ciliate<sup>-1</sup> day<sup>-1</sup> needed for maximum  
362 growth (Yih et al. 2004, Hansen & Fenchel 2006), our results suggest that abundances of free-living *T.*  
363 *amphioxiae* during the survey were too low to sustain the growth of *M. major*, leading to the decline of

364 the red water blooms. The hypothetical growth limitation of *M. major* by cryptophyte prey availability  
365 may be even stronger considering that *M. major* may compete for cryptophytes against other predators  
366 in the estuary, like dinoflagellates (Yih et al. 2004 and references therein).

367 A few different possible phenomena could enable *M. major* to proliferate in the estuary despite  
368 the low abundance of free-living *T. amphioxeia*. One explanation is that *T. amphioxeia* can replicate  
369 inside the host cell. While the ability of *T. amphioxeia* to replicate inside *M. major* has not yet been  
370 demonstrated in cultures, it has been observed in other single-celled endosymbiont-bearing organisms,  
371 such as the ciliate *Paramecium bursaria* (Kodama & Fujishima 2009, Johnson 2011). Another  
372 explanation is that *T. amphioxeia* persists inside the ciliate as a non-replicating endosymbiont for an  
373 extended period of time, and grows within the cell over the course of the bloom as *M. major* continues  
374 to graze. In the Korean isolate of the related ciliate, *M. rubrum*, it has been shown that the prey plastids  
375 can not only persist, but also maintain photosynthetic function for up to 80 days (Myung et al. 2013).  
376 These possible explanations for the differences observed between the number of free-living and  
377 ingested *T. amphioxeia* would represent a deviation from the canonical descriptions of predator-prey  
378 relationships among marine microbes (Strom 2002). However, without a cultured representative of *M.*  
379 *major*, the specifics of this predator-prey relationship remain speculative. It is clear that, while  
380 environmental conditions (such as nutrient availability) affect the physiology of *T. amphioxeia* and  
381 abundance of the cryptophyte plays a significant role in the control of the *M. major* bloom, the unique  
382 interactions between this ciliate and its cryptophyte prey contribute to *M. major*'s proliferation in  
383 estuaries.

384

### 385 **Acknowledgments**

386 Field assistance was provided by M. Wilkin and Jo Goodman. We gratefully acknowledge  
387 CMOP colleagues generally for valuable discussions on related topics. This work was supported by

388 funding from the National Science Foundation of the Science and Technology Center for Coastal  
389 Margin Observation and Prediction (CMOP) under cooperative agreement OCE-0424602.

390    **References**

391

- 392    Armstrong FAJ, Stearns CR, Strickland JDH (1967) The measurement of upwelling and subsequent  
393       biological process by means of the Technicon Autoanalyzer® and associated equipment. Deep Sea  
394       Research and Oceanographic Abstracts 14:381–389
- 395    Baptista A, Seaton C, Wilkin M, Riseman S, Needoba J, Maier D, Turner P, Kärnä T, Lopez J, Herfort  
396       L, Megler VM, Mcneil C, Crump B, Peterson T, Spitz Y, Simon H (2015) Infrastructure for  
397       collaborative science and societal applications in the Columbia River estuary. Front Earth Sci:1–24
- 398    Bergmann T, Fahnenstiel G, Lohrenz S, Millie D, Schofield O (2004) Impacts of a recurrent  
399       resuspension event and variable phytoplankton community composition on remote sensing  
400       reflectance. Journal of Geophysical Research-Oceans 109:C10S15
- 401    Carpenter EJ, Chang J (1988) Species-specific phytoplankton growth rates via diel DNA synthesis  
402       cycles. I. Concept of the method. Marine Ecology Progress Series 43:105–111
- 403    Chawla A, Jay DA, Baptista AM, Wilkin MP, Seaton C (2008) Seasonal variability and estuary-shelf  
404       interactions in circulation dynamics of a river- dominated estuary. Estuaries and Coasts 31:269–  
405       288
- 406    Crawford DW (1989) Mesodinium rubrum: the phytoplankter that wasn't. Marine Ecology Progress Series  
407       Series 58:161–174
- 408    EPA. March 1984. Nitrogen, ammonium. Method 350.1 (colorimetric, automated phenate). In Methods  
409       for Chemical Analysis of Water and Wastewater. Cincinnati, OH, USA: Environmental  
410       Monitoring and Support Laboratory, Office of Research and Development, U.S. Environmental  
411       Protection Agency.

412

413 EPA. 1997. Method 365.5. determination of orthophosphate in estuarine and coastal waters by  
414 automated colorimetric analysis. Cincinnati: National Exposure Research Laboratory Office of  
415 Research and Development U.S. Environmental Protection Agency.

416

417 Garcia Cuetos L, Moestrup O, Hansen PJ (2012) Studies on the Genus Mesodinium II. Ultrastructural  
418 and Molecular Investigations of Five Marine Species Help Clarifying the Taxonomy. *J Eukaryotic  
419 Microbiology* 59:374–400

420 Hansen PJ, Fenchel T (2006) The bloom-forming ciliate *Mesodinium rubrum* harbours a single  
421 permanent endosymbiont. *Marine Biology Research* 2:169–177

422 Herfort L, Peterson TD, Campbell V, Futrell S, Zuber P (2011) *Myrionecta rubra* (*Mesodinium  
423 rubrum*) bloom initiation in the Columbia River estuary. *Estuarine, Coastal and Shelf Science  
424* 95:440–446

425 Herfort L, Peterson TD, McCue LA, Crump BC, Prahl FG, Baptista AM, Campbell V, Warnick R,  
426 Selby M, Roegner GC, Zuber P (2011) *Myrionecta rubra* population genetic diversity and its  
427 cryptophyte chloroplast specificity in recurrent red tides in the Columbia River estuary. *Aquatic  
428 Microbial Ecology* 62:85–97

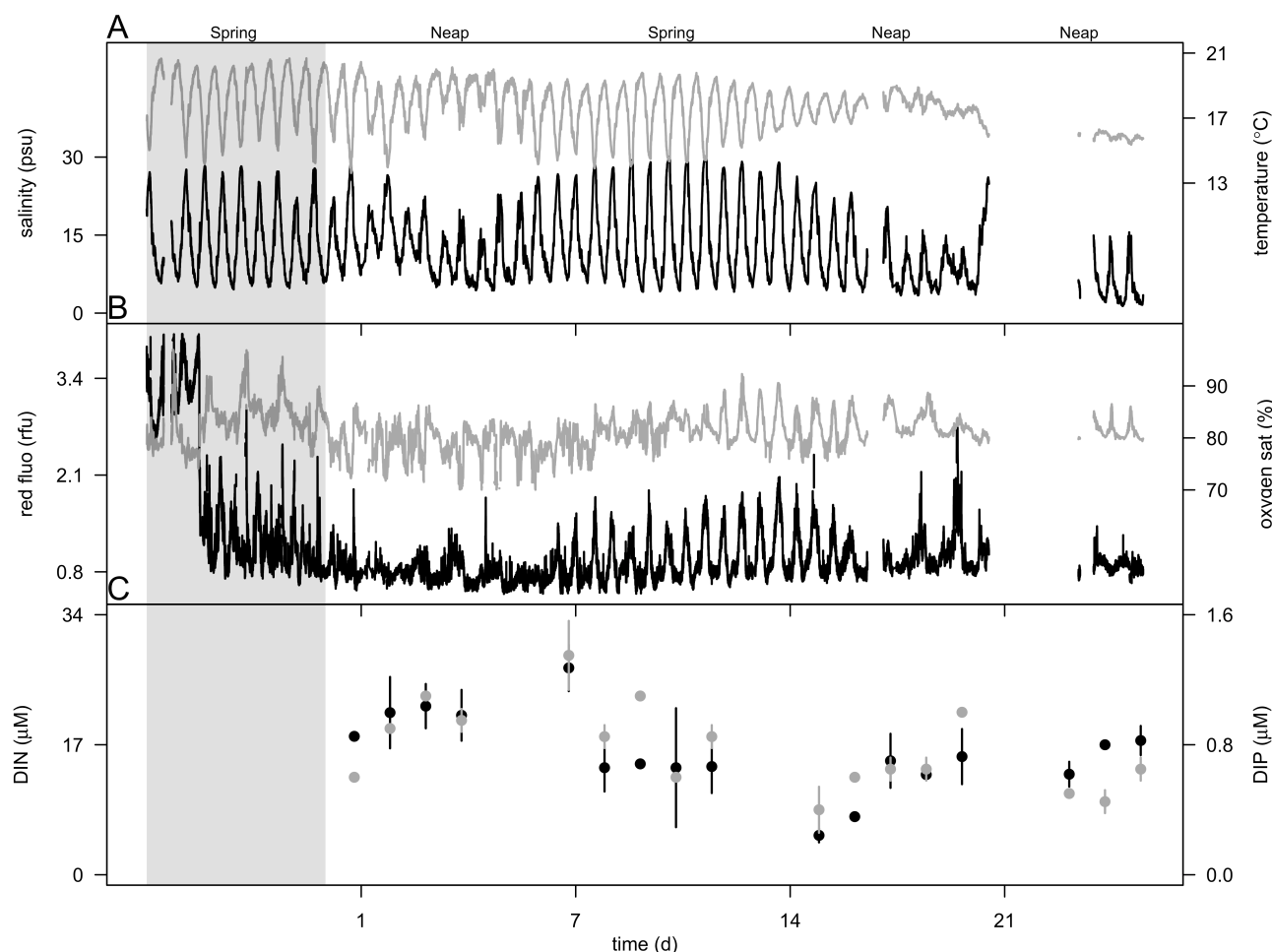
429 Herfort L, Peterson TD, Prahl FG, McCue LA, Needoba JA, Crump BC, Roegner GC, Campbell V,  
430 Zuber P (2012) Red Waters of *Myrionecta rubra* are Biogeochemical Hotspots for the Columbia  
431 River Estuary with Impacts on Primary/Secondary Productions and Nutrient Cycles. *Estuaries and  
432 Coasts* 35:878–891

433 Hunter-Cevera KR, Neubert MG, Solow AR, Olson RJ, Shalapyonok A, Sosik HM (2014) Diel size

- 434 distributions reveal seasonal growth dynamics of a coastal phytoplankton. Proceedings of the  
435 National Academy of Sciences 111:9852–9857
- 436 Jay DA, Smith JD (1990) Circulation, density distribution and neap-spring transitions in the Columbia  
437 River Estuary. Progress in Oceanography 25:81–112
- 438 Johnson MD (2011) The acquisition of phototrophy: adaptive strategies of hosting endosymbionts and  
439 organelles. Photosynthesis Research 107:117–132
- 440 Kahn P, Herfort L, Peterson TD, Zuber P (2014) Discovery of a Katablepharisspp. in the Columbia  
441 River estuary that is abundant during the spring and bears a unique large ribosomal subunit  
442 sequence element. MicrobiologyOpen 3:764–776
- 443 Kodama Y, Fujishima M (2009) Timing of perialgal vacuole membrane differentiation from digestive  
444 vacuole membrane in infection of symbiotic algae Chlorella vulgaris of the ciliate Paramecium  
445 bursaria. Protist 160:65–74
- 446 Laws EA (2013) Evaluation of In Situ Phytoplankton Growth Rates: A Synthesis of Data from Varied  
447 Approaches. Annual Review of Marine Science 5:247–268
- 448 Li B, Karl DM, Letelier RM, Bidigare RR, Church MJ (2013) Variability of chromophytic  
449 phytoplankton in the North Pacific Subtropical Gyre. Deep Sea Research Part II: Topical Studies in  
450 Oceanography 93:84–95
- 451 Lohmann H (1908) Untersuchungen zur Feststellung des vollständigen Gehaltes des Meeres an  
452 Plankton. Wissensch. Meeresuntersuchungen
- 453 Myung G, Kim HS, Park JW, Park JS, Yih W (2013) Sequestered plastids in Mesodinium rubrum are  
454 functionally active up to 80 days of phototrophic growth without cryptomonad prey. Harmful

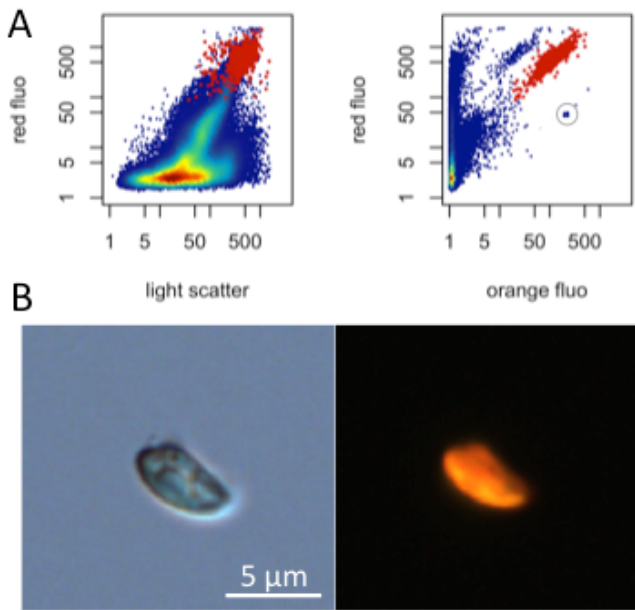
- 456 Neal VT (1972) Physical aspects of the Columbia River and its estuary (AT Pruter and DL Alverson,  
457 Eds.), University of Washington Press. The Columbia River estuary and adjacent ocean waters,  
458 Seattle, WA
- 459 Nishitani G, Nagai S, Takano Y (2008) Growth characteristics and phylogenetic analysis of the marine  
460 dinoflagellate *Dinophysis infundibulus* (Dinophyceae). Aquatic Microbial ...
- 461 Peterson TD, Golda RL, Garcia ML, Li B, Maier MA, Needoba JA, Zuber P (2013) Associations  
462 between *Mesodinium rubrum* and cryptophyte algae in the Columbia River estuary. Aquatic  
463 Microbial Ecology 68:117–130
- 464 Rial P, Garrido JL, Jaen D, Rodriguez F (2013) Pigment composition in three *Dinophysis* species  
465 (Dinophyceae) and the associated cultures of *Mesodinium rubrum* and *Teleaulax amphioxeia*.  
466 Journal of Plankton Research 35:433–437
- 467 Ribalet F, Swalwell J, Clayton S, Jiménez V, Sudek S, Lin Y, Johnson ZI, Worden AZ, Armbrust EV  
468 (2015) Light-driven synchrony of *Prochlorococcus* growth and mortality in the subtropical Pacific  
469 gyre. Proceedings of the National Academy of Sciences 112:8008–8012
- 470 Small LF, McIntire CD, MacDonald KB, Lara-Lara JR, Frey BE, Amspoker MC, Winfield T (1990)  
471 Primary production, plant and detrital biomass, and particle transport in the Columbia River  
472 Estuary. Progress in Oceanography 25:175–210
- 473 Sosik HM, Olson RJ, Neubert MG, Shalapyonok A, Solow AR (2003) Growth Rates of Coastal  
474 Phytoplankton from Time-Series Measurements with a Submersible Flow Cytometer. Limnology  
475 and Oceanography 48:1756–1765

- 476 Stoecker DK, Taniguchi A, Michaels AE (1989) Abundance of autotrophic, mixotrophic and  
477 heterotrophic planktonic ciliates in shelf and slope waters. *Marine Ecology Progress Series*  
478 50:241–254
- 479 Strom S (2002) Novel interactions between phytoplankton and microzooplankton: their influence on  
480 the coupling between growth and grazing rates in the sea. *Hydrobiologia* 480:41–54
- 481 Swalwell JE, Ribalet F, Armbrust EV (2011) SeaFlow: A novel underway flow-cytometer for  
482 continuous observations of phytoplankton in the ocean. *Limnology and Oceanography: Methods*  
483 9:466–477
- 484 van den Hoff J, Bell E (2015) The ciliate *Mesodinium rubrum* and its cryptophyte prey in Antarctic  
485 aquatic environments. *Polar Biology* 38:1305–1310
- 486 Yih W, Kim HS, Jeong HJ, Myung G, Kim YG (2004) Ingestion of cryptophyte cells by the marine  
487 photosynthetic ciliate *Mesodinium rubrum*. *Multiple values selected* 36:165–170
- 488



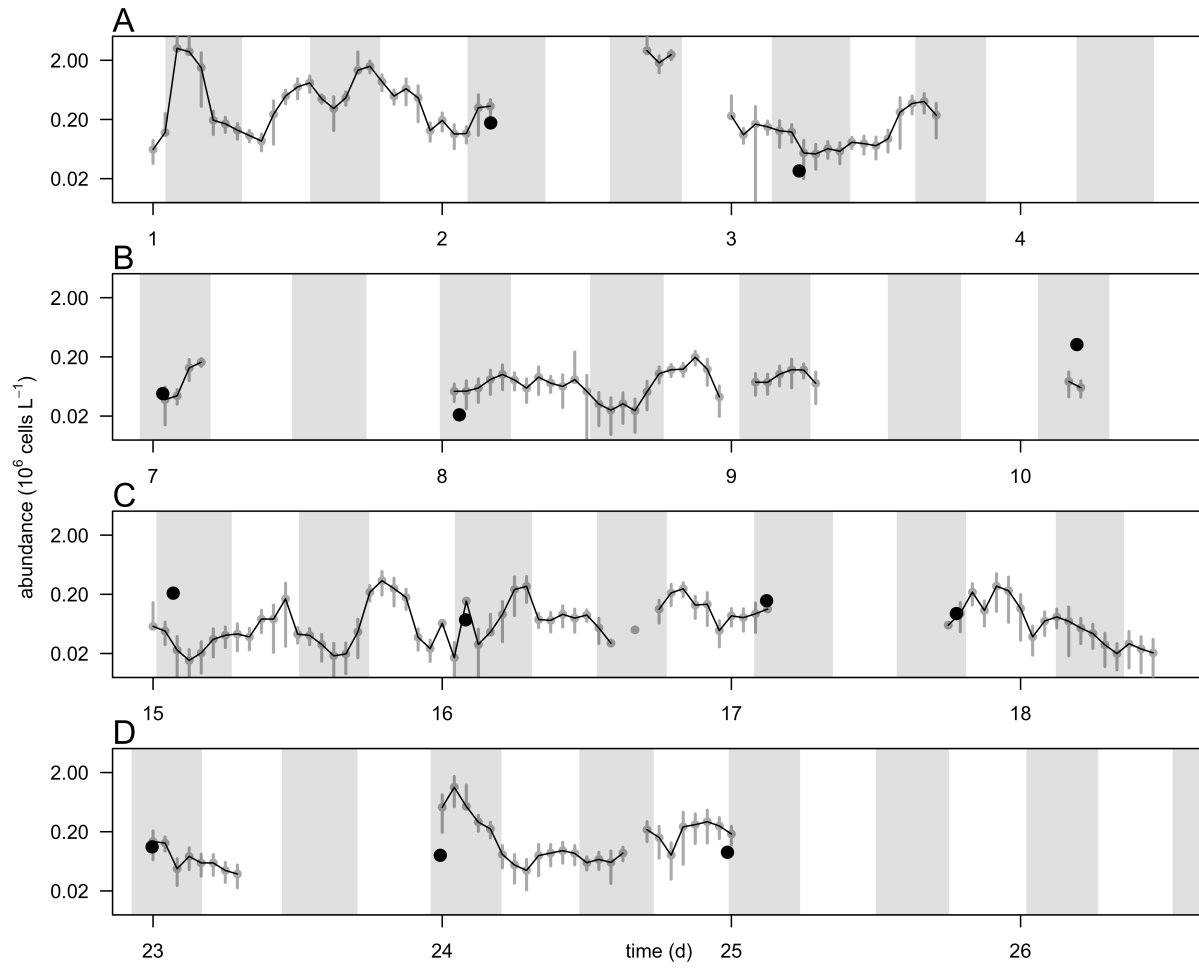
491 **Fig. 1** Hydrographic conditions prior and during the 4 week-survey in the Columbia River estuary at  
 492 2.4 m depth. A) Salinity (psu, black line) and temperature ( $^{\circ}\text{C}$ , grey line). B) Chlorophyll *a*  
 493 concentration ( $\mu\text{g L}^{-1}$ , black line) and oxygen saturation (%), grey line), and C) concentrations of  
 494 dissolved inorganic nitrogen (DIN,  $\mu\text{M}$ , open circle) and phosphorus (DIP,  $\mu\text{M}$ , black circle). Vertical  
 495 bars represent the ranges of nutrient concentrations. The grey region represents the week prior the start  
 496 of the survey.

498  
499

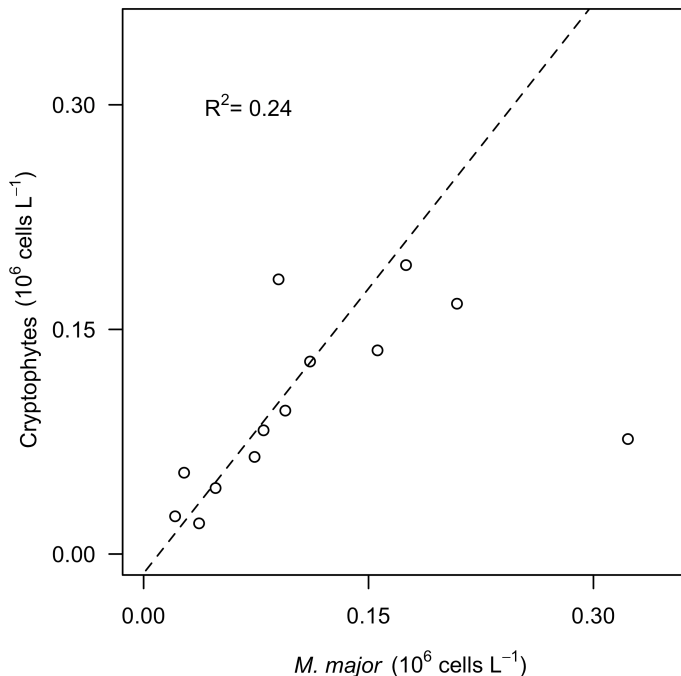


500

501 **Fig. 2** Flow cytometric signatures and micrograph of glutaraldehyde-fixed *Teleaulax*-like  
502 cryptophytes. A) Red fluorescence (692 nm wavelength) from chlorophyll versus forward light scatter  
503 (related to cell size) shows phytoplankton community structure, cryptophyte population (red dots, see  
504 right panel) and detritus (low red fluorescence) (left panel). Red fluorescence (692 nm wavelength)  
505 versus orange fluorescence (527 nm wavelength) from phycoerythrin uniquely identified a population  
506 of cryptophyte (red dots), and a tight peak of uniform fluorescent microspheres (grey circle) added as  
507 an internal standard (right panel). Cells with low orange fluorescence are the phytoplankton  
508 populations and detritus shown on the left panel. B) Micrographs using transmitted-light (left) and  
509 epifluorescence (right) microscopy after cell sorting by flow cytometry of the cryptophyte population  
510 (red dots shown in panel A). Scale bar is 5  $\mu$ m.



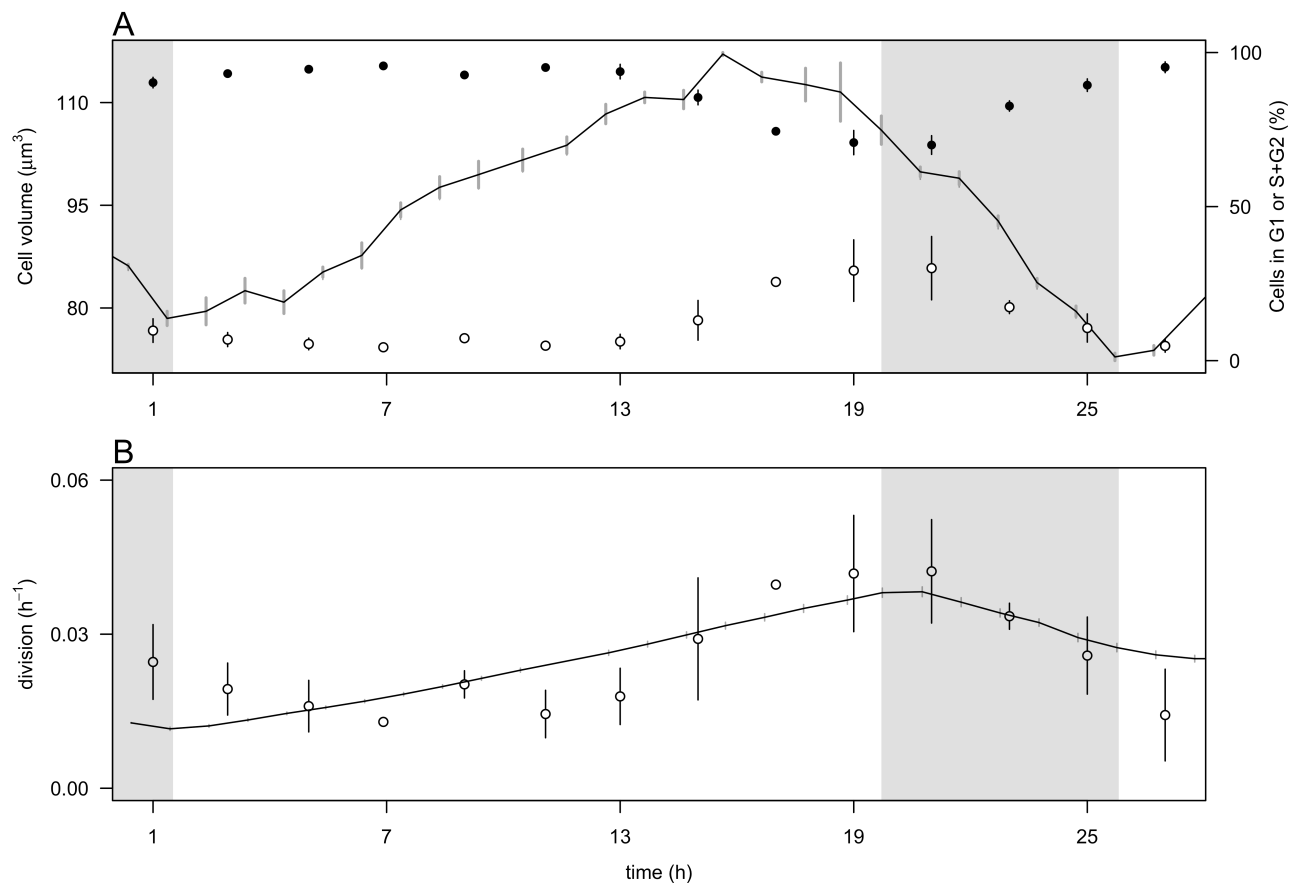
511  
 512 **Fig. 3** Hourly-averaged cell abundances of *Teleaulax*-like cryptophytes (grey circles and black line,  $10^6$   
 513 cells  $L^{-1}$ ) determined by continuous flow cytometry and abundance of *Mesodinium major* (black circles,  
 514  $10^6$  cells  $L^{-1}$ ) determined by automated microscopy from discrete samples taken during the 4-week  
 515 survey (A-D, week 1-4). Vertical bars represent the standard deviation of the hourly-mean cell  
 516 abundance of *Teleaulax*-like cryptophytes ( $n=20$ ). Grey regions represent flood tide.



517

518       **Fig. 4.** Relationship between hourly-average cell abundances of *Teleaulax*-like cryptophytes ( $10^6$   
 519       cells  $L^{-1}$ ) and *Mesodinium major* ( $10^6$  cells  $L^{-1}$ ) during the survey in the Columbia River estuary.  
 520       Dashed lines represent model II linear regression of plotted data and  $R^2$  represents the coefficient of  
 521       determination.

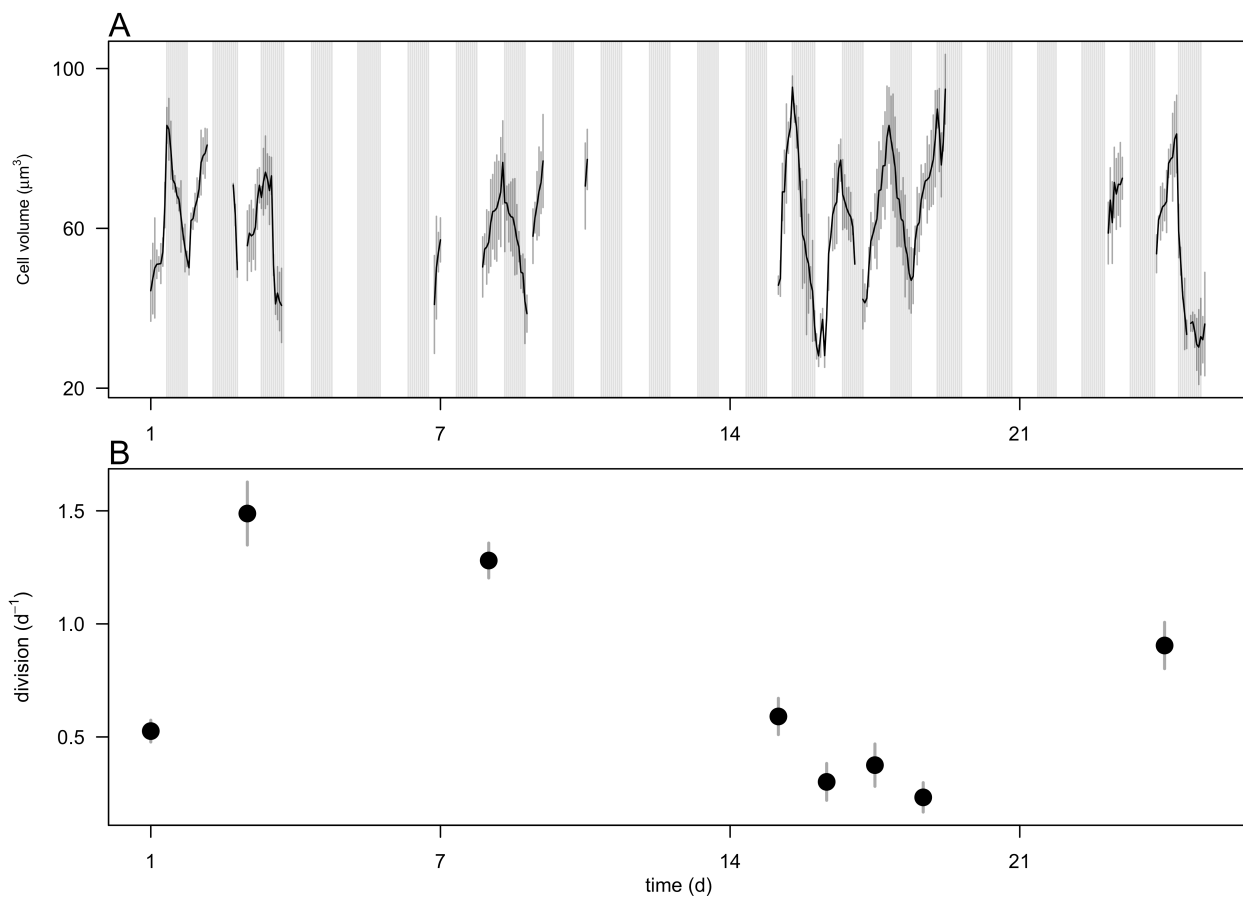
522



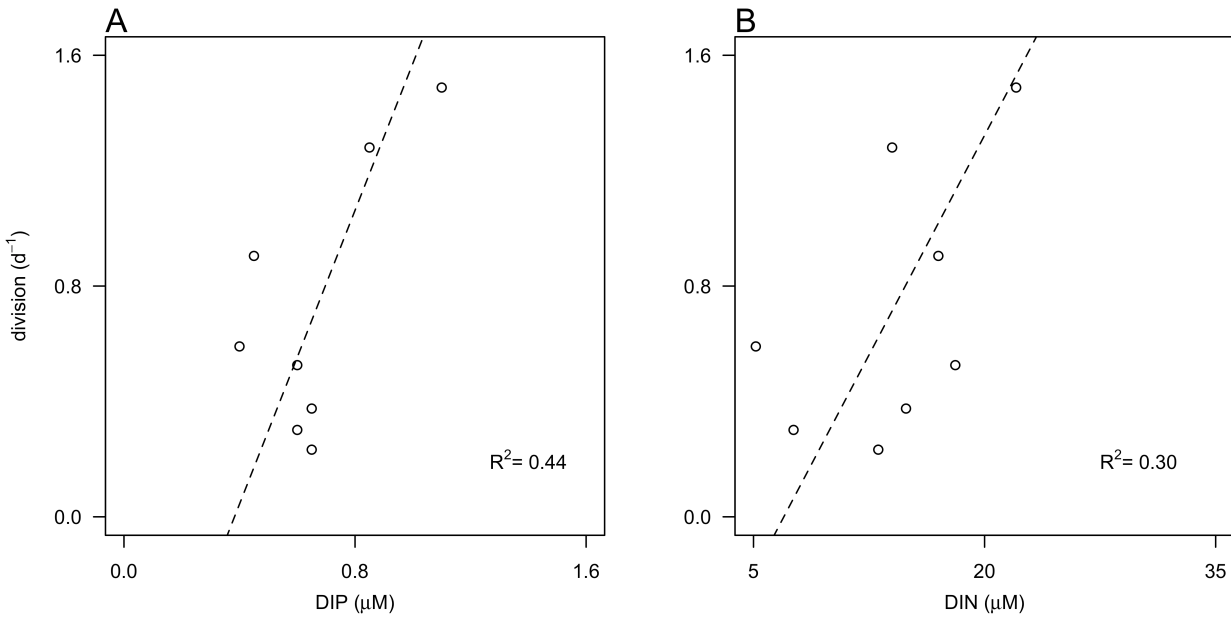
523

524 **Fig. 5.** Comparison of the size-based and cell-cycle based estimates of division rates for a cultured  
 525 cryptophyte isolate during a 28-hr experiment. A) Hourly- averaged cell volume of *Rhodomonas* sp.  
 526 ( $\mu\text{m}^3$ , black line) and percentage of cells in G1 (close circles), and S+G2 (open circles) phases. B)  
 527 Hourly division rates ( $\text{h}^{-1}$ ) based on the size distribution (black line) and on cell cycle analyses (open  
 528 circles). The grey regions indicate night. Vertical bars represent standard error (n=20 for cell volume,  
 529 n=3 for the percent of cells in G1 and S+G2 phases, n=24 for the size-based division rates).

530



533 **Fig. 6.** A) Hourly-averaged cell volumes of *Teleaulax*-like cryptophytes ( $\mu\text{m}^3$ ) estimated by flow  
 534 cytometry during the survey. Vertical grey bars represent the standard deviation of the hourly-mean  
 535 cell volume. The grey regions indicate night. B) Daily rates of cell division ( $\text{d}^{-1}$ ) of *Teleaulax*-like  
 536 cryptophytes during the survey. Vertical bars represent the propagated standard error of the sum of  
 537 hourly division rate estimates during each of the ten 24 h-period.  
 538



539

540      **Fig. 7.** Relationship between division rates ( $d^{-1}$ ) of *Teleaulax*-like cryptophytes with daily-averaged  
 541      concentrations of A) dissolved inorganic phosphate (DIP,  $\mu M$ ) and B) dissolved inorganic nitrate (DIN,  
 542       $\mu M$ ) during the survey. Dashed lines represent model II linear regression of plotted data and  $R^2$   
 543      represents the coefficient of determination.

544

545

546 *The following supplement accompanies the article*

547

548 **Dynamics of *Teleaulax* cryptophyte prey during the decline of red water blooms  
549 in the Columbia River Estuary**

550

551 Maria Hamilton, Gwenn M. Hennon, Joseph Needoba, Katie Maxey, Rhonda Morales, Tawnya  
552 Peterson, Megan Schatz, Jarred Swalwell, Peter Zuber, E. Virginia Armbrust, Francois Ribalet \*

553

554 \* Corresponding author: [ribalet@uw.edu](mailto:ribalet@uw.edu)

555 *Marine Ecology Progress Series XXX: XX–XX (201X)*

---

556 **Supplement.**

557

558

**Table**

559

560      **Table S1.** Percent of *Teleaulax amphioxiae* to the total cryptophytes during the survey, determined  
561      from the comparison of amplicons from the LSU D2 region (USE) (see Materials & Methods)

562

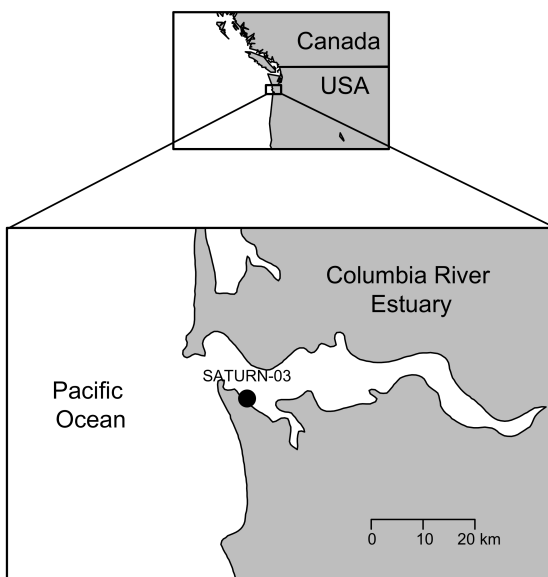
Date	% <i>T. amphioxiae</i> to total cryptophytes
9/11/13	0.40
9/13/13	0.18
9/20/13	0.06
9/24/13	0.08
10/1/13	0.23

563

564

565

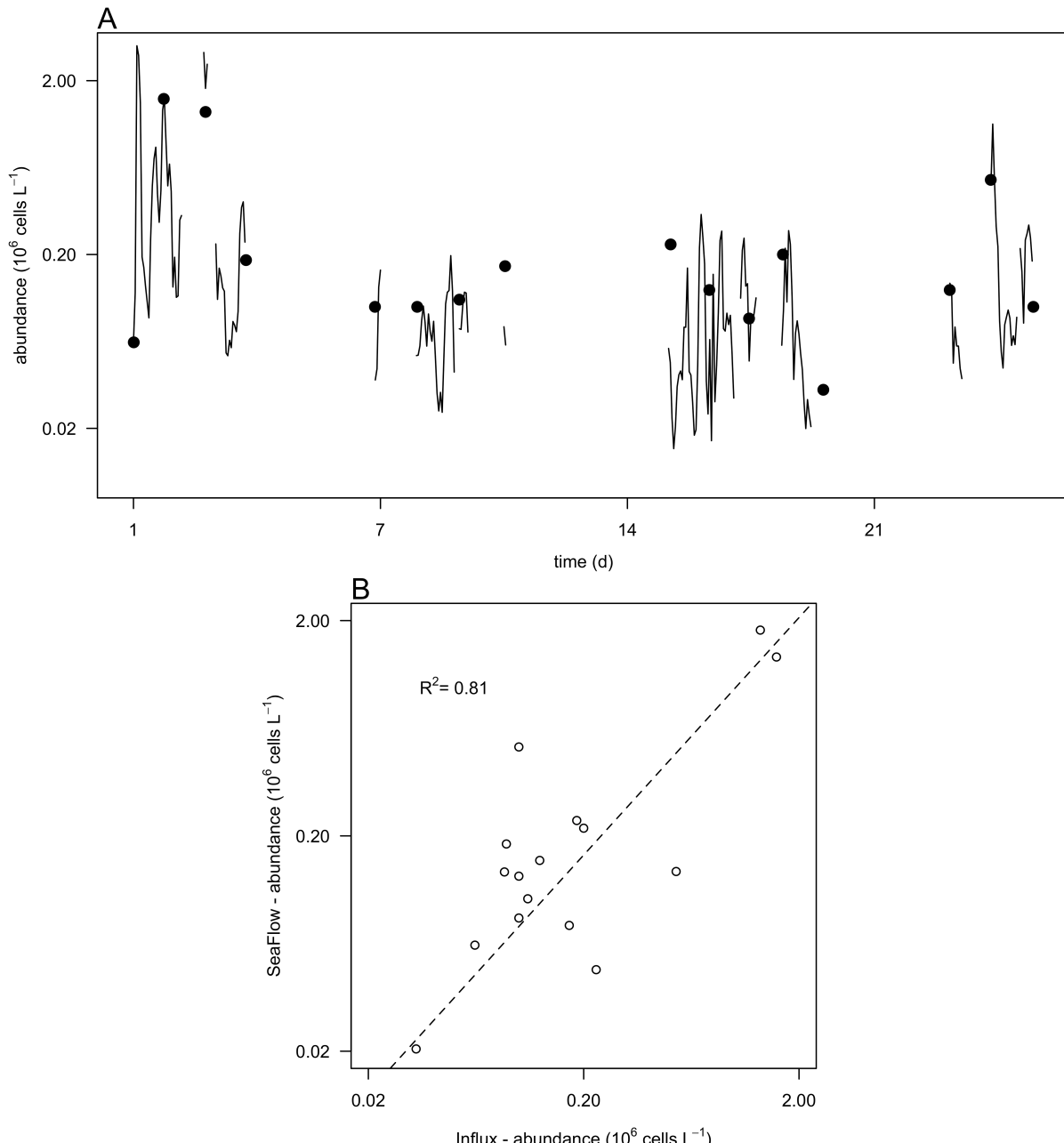
566



567

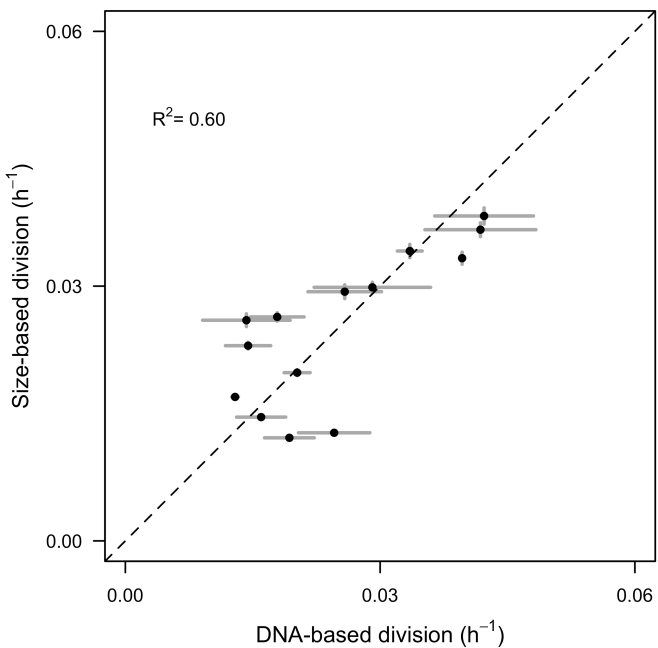
568 **Fig. S1** Map of the Columbia River Estuary with the station SATURN-03 location (black dot).

569



570

571     **Fig. S2.** Comparison of cell counts obtained with different methods. A) Cell abundances of  
 572     *Teleaulax*-like cryptophytes ( $10^6 \text{ cells L}^{-1}$ ) during the survey measured with the SeaFlow instrument  
 573     (black line) and measured with a BD Influx cell sorter (black circles). B) Correlation of cell  
 574     abundances measured by the two instruments. Dashed lines represent model II linear regression of  
 575     plotted data and  $R^2$  represents the coefficient of determination.  
 576



577

578     **Fig. S3.** Comparison of size-based division rate estimates ( $\text{h}^{-1}$ ) with DNA-based estimates of  
 579     division rates ( $\text{h}^{-1}$ ) of *Rhodomonas* sp. in cultures over the 28-hr time course experiment. Dashed lines  
 580     represent model II linear regression of plotted data and  $R^2$  represents the coefficient of determination.